A Superconducting Maglev Vehicle/Guideway System With Preview Control: Part I— Vehicle, Guideway, and Magnet Modeling

M. L. Nagurka

Department of Mechanical and
Industrial Engineering,
Marquette University,
Milwaukee, WI 53201-1881

S. K. Wang

Spacecraft Bus Electronics,
Hughes Space and
Communications Company,
2000 E. El Segundo Boulevard,
El Segundo, CA 90245-4709

Part I of this paper presents a dynamic model of magnetically-levitated (maglev) vehicle/guideway interaction. The vehicle employs a superconducting electromagnetic suspension system with canted magnets to provide simultaneous levitation and guidance in the face of guideway irregularities and cross-wind gusts. The dynamic simulation model includes a five degree-of-freedom nonlinear vehicle model, a superconducting magnet model, and a multi-span flexible guideway model. The formulation accounts for the dynamic loading on the guideway due to time-varying, distributed magnetic forces imposed by the vehicle. The maglev vehicle/guideway model is the basis for designing and testing a proposed preview control strategy in Part II of this paper.

1 Introduction

Magnetically-levitated (maglev) vehicles are one class of high-speed guided ground transportation vehicles being considered for passenger transit operation in the U.S. (Gran, 1990; Thornton, 1991). The maglev concept utilizes magnetic forces for noncontact suspension, guidance, and propulsion. Unlike conventional trains that rely on steel wheels riding on steel rails, maglev vehicles are suspended by magnetic forces, generally, on elevated guideways. In addition to levitation, magnetic forces can be employed to guide the vehicle (i.e., center it within or over the guideway), propel the vehicle along the guideway, and assist in braking action.

A goal of this study is to develop a realistic maglev vehicle/guideway interaction model. The maglev vehicle is based on Grumman's system concept (Proise et al., 1993) which uses a superconducting (SC) electromagnetic suspension (EMS) system. Combined lift and guidance is achieved by attractive forces using a single set of inclined magnets on both sides of the vehicle. This configuration reduces the number of magnets and control components and hence the vehicle weight. A nominal air gap of 40 mm between the magnet faces and guideway iron rails is proposed. This is considered a wide gap for an EMS system, and as such, a softer suspension is possible eliminating the need for a passive secondary suspension.

The model components of the maglev vehicle/guideway system are a five degree-of-freedom (DOF) vehicle model, a SC magnet model, and a flexible guideway model. In contrast to Grumman's linear vehicle model (Gran and Proise, 1993), the vehicle model here is fully nonlinear and permits large angle variations. The magnet model includes the SC magnet dynamics, which are often ignored, and employs an analytically derived magnet characteristic eliminating the need to calculate magnetic fields numerically. The magnetic force is modeled as a dynamic and continuously distributed load on a vertically flexible multiply-spanned guideway. In previous vehicle/guideway studies, the magnetic force is generally modeled as

a discontinuous multi-load (Cai et al., 1993; Wormley et al., 1992) in electrodynamic suspension (EDS) systems (that rely on repulsive forces), or simply a continuously constant load (Gran and Proise, 1993; Phelan, 1993) in EMS systems. Due to the non-negligible dynamic coupling of an EMS vehicle and a flexible guideway, the use of a dynamic and continuously distributed load model is proposed and is adopted here.

Part I of this paper develops a maglev vehicle/guideway interaction model that accounts for dynamic coupling among the magnet modules, vehicle, and guideway. This plant model is useful as a "building-block" for designing and testing control strategies. In Part II of this paper, an optimal controller with preview is proposed for the model developed here and the maglev system performance is evaluated under a number of disturbances.

2 System Model Derivations

2.1 Vehicle Model. In order to facilitate the development of a rigid-body model for the maglev vehicle, two coordinate systems are introduced: an inertial coordinate frame and a carbody coordinate frame. As shown in Fig. 1, the origin of the inertial coordinate frame coincides with the vehicle CG when the vehicle is in its nominal position. The carbody motion is then described by the translational and rotational transformations between these two coordinate systems. The carbody coordinate frame is fixed in the vehicle carbody with principal axes X_C, Y_C, and Z_C and origin located at the vehicle center of gravity identified as CG. The inertial coordinate frame, $X_I Y_I Z_I$, is assumed to move along the guideway longitudinal direction (i.e., X_I direction) at constant vehicle speed, V_v.

Since vehicle acceleration (and braking) is not addressed, the vehicle motion can be characterized by the lateral and vertical displacements of the carbody CG and the roll, pitch, and yaw angles which describe the orientation of the carbody coordinate frame with respect to the inertial coordinate frame. The lateral and vertical displacements of the carbody CG are denoted by y_c and z_c, respectively. It is assumed that the carbody axes are initially aligned with the inertial reference axes. Then, the orientation of the carbody frame can be reached by successive rotations as follows: (*i*) ψ_c (yaw) about the Z_C axis, (*ii*) θ_c
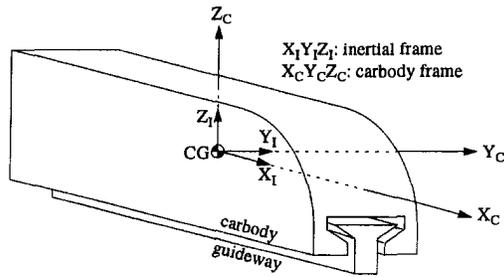
Fig. 1 Inertial and carbody coordinate frames in nominal position

(pitch) about the resulting Y_C axis, and (iii) ϕ_c (roll) about the resulting X_C axis.

Figure 2 shows the vehicle configuration in its nominal position. There are an even number, N_m, of magnet modules on each side inclined at angle β from vertical. By design, β is selected so that the magnetic forces pass through the longitudinal axis of the vehicle when the vehicle is in its nominal position. Each module contains several magnets controlled as a group. For instance, in the Grumman baseline design each module houses two magnets with twelve modules on each side of the vehicle (Proise et al., 1993). The magnetic force from each magnet module is assumed to be distributed uniformly along the module length, l_m. The vehicle length and height are denoted by L_v and h_v, respectively. Also shown in the figure are the nominal air gap, h_0, and the height and width between the module and the carbody CG, denoted by h_c and w_c, respectively.

As indicated in Fig. 2, the vehicle is supported by magnetic forces from two rows of magnet modules under the carbody. In addition, the vehicle may be disturbed by a cross-wind gust represented by an aerodynamic force, F_w, in the lateral (Y_I) direction and an aerodynamic moment, M_w, in the yaw (Z_I) direction.

The derivation of the equations of motion consists of three steps: (i) identification of the air gap at each module, (ii) determination of the resultant magnetic force and corresponding moment, and (iii) application of Newton's second law and Euler's equations.

2.1.1 Air Gap. Figure 3 shows the cross-section of the vehicle relative to the guideway in a general position, where both the vehicle and guideway are displaced from their nominal positions. (The nominal guideway position is indicated by the dashed lines, and the guideway is shown deflected in both vertical and horizontal directions.) In Fig. 3, point a is the centroid of the jth magnet module ($j = 1, \ldots, N_m$). Point b is the rail center at the cross-section of module j when the vehicle and the guideway are both in their nominal positions. Point c is the
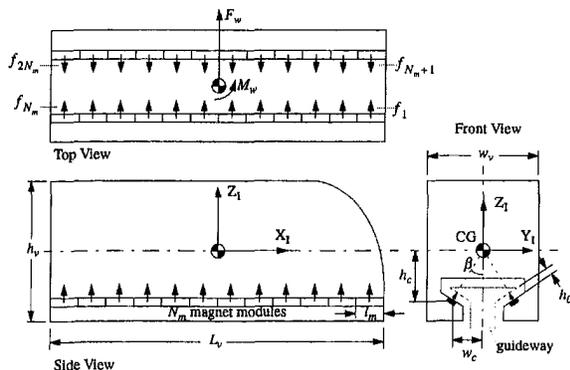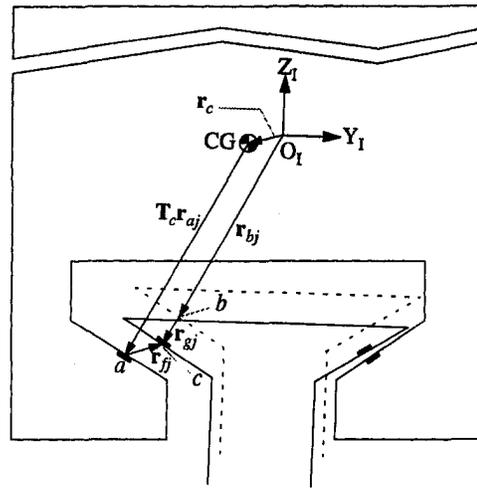

Fig. 2 Vehicle configuration

Fig. 3 Cross-section showing general vehicle/guideway position

rail center after the guideway is displaced, and is located in the same lateral-vertical plane as point b. In general, points a and c are not in the same lateral-vertical plane unless the pitch and yaw angles are both zero. From Fig. 3, the relative displacement from point a to point c can be expressed in the inertial coordinate frame as

$$\mathbf{r}_{fj} = -\mathbf{T}_c \mathbf{r}_{aj} - \mathbf{r}_c + \mathbf{r}_{bj} + \mathbf{r}_{gj} \qquad (1)$$

where, using the notation $s\alpha = \sin \alpha$ and $c\alpha = \cos \alpha$,

$$\mathbf{T}_c = \begin{bmatrix} c\theta_c c\psi_c & s\phi_c s\theta_c c\psi_c - c\phi_c s\psi_c & c\phi_c s\theta_c c\psi_c + s\phi_c s\psi_c \\ c\theta_c s\psi_c & s\phi_c s\theta_c s\psi_c + c\phi_c c\psi_c & c\phi_c s\theta_c s\psi_c - s\phi_c c\psi_c \\ -s\theta_c & s\phi_c c\theta_c & c\phi_c c\theta_c \end{bmatrix}$$

$$(2)$$

$$\mathbf{r}_{aj} = \begin{bmatrix} l_m[(N_m + 1)/2 - j] \\ -w_c \\ -h_c \end{bmatrix},$$

$$\mathbf{r}_{a(N_m+j)} = \begin{bmatrix} l_m[(N_m + 1)/2 - j] \\ w_c \\ -h_c \end{bmatrix}, \quad j = 1, \ldots, N_m \quad (3)$$

$$\mathbf{r}_{bj} = \begin{bmatrix} l_m[(N_m + 1)/2 - j] \\ -w_c + h_0 \sin \beta \\ -h_c + h_0 \cos \beta \end{bmatrix},$$

$$\mathbf{r}_{b(N_m+j)} = \begin{bmatrix} l_m[(N_m + 1)/2 - j] \\ w_c - h_0 \sin \beta \\ -h_c + h_0 \cos \beta \end{bmatrix}, \quad j = 1, \ldots, N_m \quad (4)$$

$$\mathbf{r}_c = [0, y_c, z_c]^T, \quad \mathbf{r}_{gj} = [0, y_{gj}, z_{gj}]^T,$$

$$j = 1, \ldots, 2N_m \quad (5), (6)$$

$\mathbf{T}_c$ is a roll-pitch-yaw transformation matrix which converts a vector from the carbody coordinate frame to the inertial coordinate frame. $\mathbf{r}_{aj}$ is the vector from the carbody CG to module j in the carbody coordinate frame. $\mathbf{r}_{bj}$ is the vector from the origin of the inertial frame to point b for each module j. $\mathbf{r}_c$ is the displacement of the carbody CG. Note that the longitudinal component of $\mathbf{r}_c$ is zero since the carbody CG moves at the same speed as the inertial coordinate frame along the X_I direction. $\mathbf{r}_{gj}$ in Eq. (6) is the guideway deviation vector where y_{gj} and z_{gj} are the guideway deviations observed at module j in the lateral and vertical directions, respectively. Since points b and c are

in the same lateral-vertical plane, the longitudinal component of $\mathbf{r}_{gj}$ is zero.

The air gap vector is defined as the components of $\mathbf{r}_{fj}$ in the Y_I and Z_I directions. It follows that the air gap can be expressed as

$$h_j = |[0, \mathbf{r}_{fj} \cdot \mathbf{u}_y, \mathbf{r}_{fj} \cdot \mathbf{u}_z]^T|, \quad j = 1, \ldots, 2N_m \quad (7)$$

where $\mathbf{u}_y$ and $\mathbf{u}_z$ are unit vectors in the Y_I and Z_I directions, respectively.

2.1.2 Resultant Magnetic Force and Moment. Since the magnetic force that provides guidance and levitation has the same direction as the air gap vector, the magnetic force and resulting moment about the carbody CG can be represented by

$$\mathbf{F}_j = f_j[0, \mathbf{r}_{fj} \cdot \mathbf{u}_y, \mathbf{r}_{fj} \cdot \mathbf{u}_z]^T/h_j, \quad \mathbf{M}_j = \mathbf{T}_c^T(\mathbf{T}_c \mathbf{r}_{aj} \times \mathbf{F}_j),$$

$$j = 1, \ldots, 2N_m \quad (8), (9)$$

In Eq. (8), f_j is the magnitude of the magnetic force at module j. This force is provided by the magnet module and is adjusted by the control system (described in Part II). The total magnetic force and moment applied to the carbody CG can be expressed as

$$[F_x, F_y, F_z]^T = \sum_{j=1}^{2N_m} \mathbf{F}_j, \quad [M_x, M_y, M_z]^T = \sum_{j=1}^{2N_m} \mathbf{M}_j \quad (10), (11)$$

where F_x, F_y, and F_z are the resultant force components in the X_I, Y_I, and Z_I directions, respectively, and M_x, M_y, and M_z are the resultant moment components in the X_C, Y_C, and Z_C directions, respectively.

2.1.3 Equations of Motion. In the vehicle model, the carbody is subjected to a cross-wind gust that applies an equivalent side force, F_w, and a yaw moment, M_w, upon the carbody CG. With knowledge of the resultant magnetic force and associated moment, the vehicle model equations of motion can be written as

$$F_y + F_w = M_v \ddot{y}_c, \quad F_z - M_v g = M_v \ddot{z}_c, \quad (12), (13)$$

$$M_x = I_x \dot{\omega}_x - (I_y - I_z)\omega_y \omega_z \quad (14)$$

$$M_y = I_y \dot{\omega}_y - (I_z - I_x)\omega_z \omega_x, \quad (15)$$

$$M_z + M_w = I_z \dot{\omega}_z - (I_x - I_y)\omega_x \omega_y \quad (16)$$

$$\dot{\phi}_c = \omega_x + (\omega_y \sin \phi_c + \omega_z \cos \phi_c) \tan \theta_c, \quad (17)$$

$$\dot{\theta}_c = \omega_y \cos \phi_c - \omega_z \sin \phi_c \quad (18)$$

$$\dot{\psi}_c = (\omega_y \sin \phi_c + \omega_z \cos \phi_c)/\cos \theta_c \quad (19)$$

where g is the acceleration due to gravity, and ω_x, ω_y, and ω_z are the roll, pitch, and yaw angular velocities, respectively, in the carbody coordinate frame. Equations (12) and (13) are the lateral and vertical translational equations of motion given by Newton's second law. Equations (14)–(16) are the rotational equations of motion from Euler's equations. Equations (17)–(19) are the angle-angular velocity relations which couple the vehicle angular velocities to the roll, pitch, and yaw angles.

In summary, the vehicle dynamics can be characterized by Eqs. (12)–(19). The control input is the magnetic force f_j at magnet module j, which is set up by the SC magnets in the module and adjusted by a control law. The disturbance inputs contain the force, F_w, and moment, M_w, due to cross-wind gusts and the guideway deviation, $\mathbf{r}_{gj}$, observed at each magnet module. The outputs of the vehicle model include the air gap, h_j, at each module determined by Eq. (7).
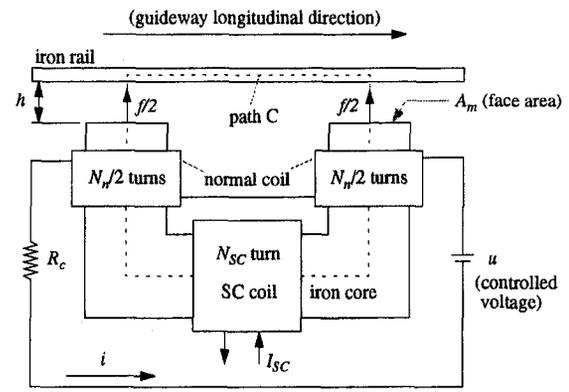
Fig. 4   Single superconducting magnet

2.2 SC Magnet Model. A single SC magnet, shown schematically in Fig. 4, is attracted to a guideway iron rail and consists of an iron-core magnet, a SC coil wrapped on the back leg of the iron core, and a set of serially connected normal coils attached to both pole ends of the iron core. N_{SC} and N_n are the number of turns in the SC coil and the normal coils, respectively. The current in the SC coil is I_{SC}. The trim current, i, in the normal coils is driven by a controlled voltage, u, to maintain the air gap, h, at its nominal value. The resistance of the normal coil is denoted by R_c and the face area of each magnetic pole is denoted by A_m.

In Fig. 4, the attractive force, f, set up by the magnetic flux density, B_m, in the air gap is

$$f = \frac{B_m^2 A_m}{\mu_0}, \quad B_m = \frac{\mu_0}{2h}(N_{SC}I_{SC} + N_n i) \quad (20), (21)$$

where μ_0 denotes the permeability of air. In Eq. (20), f can be derived using the law of conservation of energy for the magnetic energy stored in the air gap (e.g., Iskander, 1992). In Eq. (21), B_m can be obtained by applying Ampere's law along path C in Fig. 4. Also, it is assumed that (*i*) the leakage flux in the iron rail and iron core is negligible and (*ii*) the air gap is sufficiently narrow such that the total flux in the iron core flows across the gap without loss and the force that develops is normal to the gap (i.e., no edge effects). To minimize the leakage flux, special magnetic pole arrangements can be employed (Kalsi et al., 1993).

The SC current, I_{SC}, provides lifting capability to compensate for the vehicle weight and is assumed constant in this study. The trim current, i, is achieved by a power supply with controlled voltage, u. From Kirchhoff's voltage law, the relation between the trim current and the controlled voltage, u, is

$$u - R_c i - N_n \frac{d(B_m A_m)}{dt} = 0 \quad (22)$$

In Eq. (22), the last term on the left-hand side is the electromotive force (emf) induced by the normal coil. (The emf induced by the SC coil is absent since constant SC current is assumed.)

For a magnet module housing n_m SC magnets, the magnetic force in each magnet is generated by the same power supply and the total magnetic force is n_m times the force set up by a single magnet. Thus, the magnetic force generated by each module can be written as

$$f_j = \frac{\mu_0 A_m n_m}{4h_j^2}(N_{SC}I_{SC} + N_n i_j)^2 \quad (23)$$

for $j = 1, \ldots, 2N_m$, where h_j is the air gap at the jth module and the trim current, i_j, of module j is determined from the voltage Eq. (22) as
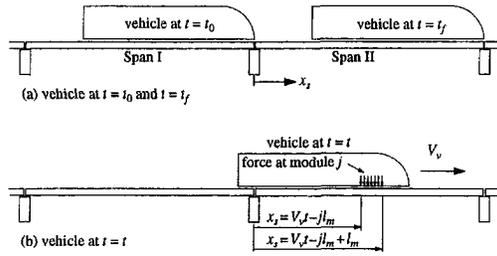
Fig. 5 Vehicle traversing guideway spans

$$u_j = R_c i_j + \frac{\mu_0 A_m N_n^2}{2h_j} \frac{di_j}{dt} - \frac{\mu_0 A_m N_n (N_{SC} I_{SC} + N_n i_j)}{2h_j^2} \frac{dh_j}{dt} \quad (24)$$

for $j = 1, \ldots, 2N_m$, with u_j being the controlled voltage for the jth module.

In summary, the dynamics of the SC magnet model are described by the voltage Eq. (24) for each module and can be represented by $2N_m$ first-order ordinary differential equations (ODEs). The resulting trim current and the constant SC current in each magnet module produce a magnetic flux which sets up the attractive magnetic force between the iron core and the iron rail. The magnetic force at each module, described by Eq. (23), is a nonlinear function of the trim current, SC current, and air gap.

2.3 Guideway Model. A Bernoulli-Euler beam with simply supported ends is used to model each elevated guideway span. The equation of motion for a span can be expressed as

$$EI \frac{\partial^4}{\partial x_s^4} \tilde{w}_s(x_s, t) + c \frac{\partial}{\partial t} \tilde{w}_s(x_s, t) + \gamma \frac{\partial^2}{\partial t^2} \tilde{w}_s(x_s, t)$$
$$= \tilde{f}(x_s, t) \quad (25)$$

where x_s is the span axial coordinate, EI is the bending rigidity, c is the viscous damping coefficient, γ is the span mass per unit length, $\tilde{w}_s(x_s, t)$ is the span vertical deflection, and $\tilde{f}(x_s, t)$ is the vertical loading force per unit length due to the moving vehicle. (The use of the superscript $\sim$ denotes functional dependence on both space and time.) This guideway model accounts only for span vertical deflections. Future guideway models may incorporate lateral as well as torsional deflections.

The vehicle/guideway interaction is considered in the time interval $[t_0, t_f]$ as depicted in Fig. 5(a). At $t = t_0$, the vehicle is completely located on Span I and just about to enter Span II. As time increases, the vehicle load excites both Span I and Span II simultaneously. In this study, it is assumed that the vehicle length, L_v, is less than the guideway span length, L_s. As a result, the vehicle is completely located on Span II at $t = t_f$. For multi-span configurations, additional spans are "daisy-chained," i.e., at $t = t_f$, the clock is reset to $t = t_0$ and the algorithm for the following span is re-applied (Cherchas, 1979). The process for deriving the vehicle/guideway interaction involves three steps. The first step is to convert the magnetic forces on the modules into the distributed loading forces on Span I and Span II. The second step is to solve for the distributed span deflections. The final step is to obtain the guideway deflection observed at each module.

2.3.1 Distributed Loading Forces. The dynamic loading on Span II is considered first. Figure 5(b) depicts the distributed loading force of module j moving along Span II at vehicle speed V_v. At time t, the front and rear of module j (for $j = 1, \ldots, N_m$) are located at $x_s = V_v t - jl_m + l_m$ and $x_s = V_v t - jl_m$, respectively, where x_s is the axial coordinate for Span II. Since the magnets are inclined at an angle β, the distributed load per unit length in the vertical direction is given by $f_j \cos \beta / l_m$. The

profile of the loading force at each module is a square wave which can be expressed as

$$\tilde{f}_{II,j}(x_s, t) = [u_s(V_v t - jl_m, x_s)$$
$$- u_s(V_v t - jl_m + l_m, x_s)] f_j \cos \beta / l_m \quad (26)$$

$$\tilde{f}_{II,j+N_m}(x_s, t) = [u_s(V_v t - jl_m, x_s)$$
$$- u_s(V_v t - jl_m + l_m, x_s)] f_{j+N_m} \cos \beta / l_m \quad (27)$$

for $j = 1, \ldots, N_m$, where subscript II denotes that the force acts on Span II and u_s is the unit step function defined by

$$u_s(x_{s0}, x_s) = \begin{cases} 1, & x_s \geq x_{s0} \\ 0, & x_s < x_{s0} \end{cases} \quad (28)$$

Similarly, the profile of the loading force at each module on Span I can be expressed as

$$\tilde{f}_{I,j}(-x_s, t) = \tilde{f}_{II,j}(x_s, t), \quad (29)$$

$$\tilde{f}_{I,j+N_m}(-x_s, t) = \tilde{f}_{II,j+N_m}(x_s, t) \quad (30)$$

for $j = 1, \ldots, N_m$ and $x_s < 0$. The total loading force for Spans I and II is the summation of the individual loading forces and can be represented as

$$\tilde{f}_I(-x_s, t) = \sum_{j=1}^{2N_m} \tilde{f}_{I,j}(-x_s, t), \quad (31)$$

$$\tilde{f}_{II}(x_s, t) = \sum_{j=1}^{2N_m} \tilde{f}_{II,j}(x_s, t) \quad (32)$$

2.3.2 Distributed Span Deflections. To determine the distributed span deflections, a modal analysis method is utilized in which the span deflections on Spans I and II can be expressed as

$$\tilde{w}_I(-x_s, t) = \sum_{j=1}^{n_s} a_j(t) \sin(-j\pi x_s / L_s), \quad (33)$$

$$\tilde{w}_{II}(x_s, t) = \sum_{j=1}^{n_s} b_j(t) \sin(j\pi x_s / L_s) \quad (34)$$

where n_s is the number of mode shapes and $a_j(t)$ and $b_j(t)$ are the modal amplitudes for Spans I and II, respectively, and can be determined by

$$\ddot{a}_j(t) + \frac{c}{\gamma} \dot{a}_j(t) + \frac{EI}{\gamma} \left(\frac{j\pi}{L_s}\right)^4 a_j(t)$$
$$= \frac{2}{\gamma L_s} \int_{-L_s}^{0} \tilde{f}_I(-x_s, t) \sin\left(\frac{-j\pi x_s}{L_s}\right) dx_s \quad (35)$$

$$\ddot{b}_j(t) + \frac{c}{\gamma} \dot{b}_j(t) + \frac{EI}{\gamma} \left(\frac{j\pi}{L_s}\right)^4 b_j(t)$$
$$= \frac{2}{\gamma L_s} \int_{0}^{L_s} \tilde{f}_{II}(x_s, t) \sin\left(\frac{j\pi x_s}{L_s}\right) dx_s \quad (36)$$

for $j = 1, \ldots, n_s$. Since the loading forces in Eqs. (33) and (34) are both staircase functions, the integrals on the right-hand sides of Eqs. (35) and (36) can be solved analytically (Wang, 1995).

2.3.3 Guideway Deflection at Each Module. To find the guideway deflection at each magnet module, the location of each module is identified first. At time t, the centroid location of each magnet module can be represented as
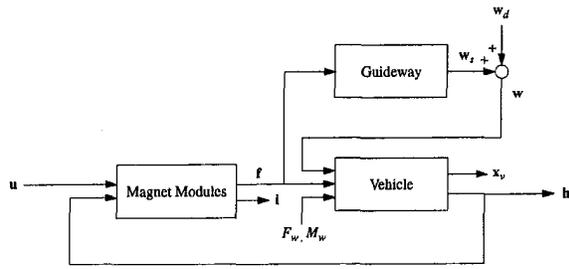
Fig. 6   Block diagram of maglev system (without controller)

$$x_{s,j} = x_{s,j+N_m} = V_v t - j l_m + l_m/2 \qquad (37)$$

for $j = 1, \ldots, N_m$, where $x_{s,j}$ denotes the location of the centroid of module j. Since the magnetic forces applied to the guideway rails are distributed, the effective guideway displacement at each module is given by the average guideway displacement over the module length (Gran and Proise, 1993). The magnet module may be located entirely on Span I, on both Span I and Span II, or entirely on Span II. The corresponding deflections can be represented as

$$w_{s,j}(t) = w_{s,j+N_m}(t) = \begin{cases} \dfrac{1}{l_m} \displaystyle\int_{x_{s,j}-l_m/2}^{x_{s,j}+l_m/2} \tilde{w}_{\mathrm{I}}(-\sigma, t)d\sigma, & x_{s,j} \le -\dfrac{l_m}{2} \\[4mm] \dfrac{1}{l_m} \left[\displaystyle\int_{x_{s,j}-l_m/2}^{0} \tilde{w}_{\mathrm{I}}(-\sigma, t)d\sigma + \displaystyle\int_{0}^{x_{s,j}+l_m/2} \tilde{w}_{\mathrm{II}}(\sigma, t)d\sigma \right], & -\dfrac{l_m}{2} < x_{s,j} < \dfrac{l_m}{2} \quad (38) \\[4mm] \dfrac{1}{l_m} \displaystyle\int_{x_{s,j}-l_m/2}^{x_{s,j}+l_m/2} \tilde{w}_{\mathrm{II}}(\sigma, t)d\sigma, & x_{s,j} \ge \dfrac{l_m}{2} \end{cases}$$

In summary, the magnetic forces (per length) due to the vehicle/guideway interaction are described by Eqs. (26)–(38). Equations (31) and (32) convert these magnetic forces into distributed loading forces on Span I and Span II. The distributed span deflections are then solved via Eqs. (35) and (36). Finally, the guideway deflection observed at each magnet module is obtained from Eq. (38).

The input to the guideway model is the magnetic force at each magnet module and the output is the corresponding guideway deflection. The guideway dynamic analysis considers the first n_s modes of beam vibration. The guideway model accounts for two sequential spans which are concatenated for guideways involving more spans. Since each span requires n_s second-order ODEs, the governing equations consist of $2n_s$ second-order ODEs for two spans.

2.4   Combined Maglev Model. The block diagram of Fig. 6 depicts the interaction among the dynamic models for the maglev vehicle, SC magnet, and guideway, and represents the maglev system without a controller. The controlled variables are the applied voltage, $\mathbf{u}$,

$$\mathbf{u} = [u_1, \ldots, u_{2N_m}]^T \qquad (39)$$

where u_j ($j = 1, \ldots, 2N_m$) are specified by a control law (described in Part II). The maglev vehicle is subject to aerodynamic effects, represented by F_w, and M_w, and to guideway deviation, $\mathbf{w}$. This deviation, $\mathbf{w}$, is the superposition of the guideway deflection, $\mathbf{w}_s$, and the guideway irregularity, $\mathbf{w}_d$,

$$\mathbf{w}_s = [0, \ldots, 0, w_{s,1}, \ldots, w_{s,2N_m}]^T, \qquad (40)$$

$$\mathbf{w}_d = [w_{dy,1}, \ldots, w_{dy,2N_m}, w_{dz,1}, \ldots, w_{dz,2N_m}]^T \qquad (41)$$

where $w_{s,j}$ ($j = 1, \ldots, 2N_m$) is the guideway vertical deflection

obtained from Eq. (38), and $w_{dy,j}$ and $w_{dz,j}$ ($j = 1, \ldots, 2N_m$) are the lateral and vertical guideway irregularities, respectively, due to random manufacturing and construction practice, settlement, etc. The state variables include the trim current, $\mathbf{i}$, and the vehicle state, $\mathbf{x}_v$,

$$\mathbf{i} = [i_1, \ldots, i_{2N_m}]^T \qquad (42)$$

$$\mathbf{x}_v = [y_c, z_c, \phi_c, \theta_c, \psi_c, \dot{y}_c, \dot{z}_c, \omega_x, \omega_y, \omega_z]^T \qquad (43)$$

where i_j ($j = 1, \ldots, 2N_m$) is solved from Eq. (24), and $\mathbf{x}_v$ is the solution of the vehicle equations of motion (12)–(19). The output is the air gap vector, $\mathbf{h}$,

$$\mathbf{h} = [h_1, \ldots, h_{2N_m}]^T \qquad (44)$$

where h_j ($j = 1, \ldots, 2N_m$) is determined by Eq. (7).

The model derived in this paper is nonlinear and coupled. The guideway deflection dynamics, Eqs. (35) and (36), involve the loading forces, $\hat{f}_{\mathrm{I}}$ and $\hat{f}_{\mathrm{II}}$, which are linked to the magnetic forces, f_j, by Eqs. (26) and (27). Also, the vehicle dynamics, equations (12)–(16), are driven by the magnetic forces which are themselves coupled to the air gaps, h_j, via Eqs. (8) and (23).

3   Conclusion

A detailed dynamic model for simulating a SC EMS-type maglev vehicle operating at constant forward speed over a multi-span elevated flexible guideway subject to cross-wind gust and guideway irregularities is developed. The components of the maglev model include a five DOF vehicle model, a nonlinear SC magnet system, and a flexible guideway model:

- The vehicle model considers a single carbody travelling horizontally at constant speed with DOFs in the lateral, vertical, roll, pitch, and yaw directions. The vehicle model accepts magnetic forces (assumed uniformly distributed for each module) as inputs and is subject to guideway disturbances and aerodynamic loading. Future models may consider multi-car consists and the effects of carbody flexibility, propulsion, and braking.

- The SC magnet system consists of magnet modules which accept input signals from a controller (the topic of Part II) to provide magnetic forces for levitating and guiding the vehicle. The forces are generated from magnetic fields set up by the SC and normal coils in the magnet modules. Assumptions include negligible loss of magnetic flux and constant current in the SC coils. To satisfy the first assumption, the maximum air gap is limited. To relax the second assumption, a control system for regulating the SC current could be included in future models.

- The guideway model determines the vertical deflection of the spans observed by each magnet module. It is assumed that each span is simply supported. Further, the vehicle length is assumed to be less than the span length such that only the dynamics of two sequential spans need to be considered. The guideway loading is modeled as a dynamic and continuously distributed force to account

642 / Vol. 119, DECEMBER 1997

for the dynamic coupling between the vehicle and the guideway spans. The guideway model may be extended in the future to handle vehicle motion in a curved guideway section, guideway torsional and lateral dynamics, and different boundary conditions for the spans.

To complete the maglev model, controller models are necessary. An optimal preview control scheme is proposed in Part II, and the performance of the comprehensive maglev model is then studied in detail.

Acknowledgment

References

Cai, Y., Chen, S. S., Rote, D. M., and Coffey, H. T., 1993, "Vehicle/Guideway Interaction and Ride Comfort in Maglev Systems," *Proceedings of the International Conference on Speedup Technology for Railway and Maglev Vehicles,* Vol. I, Nov. 22–26, Yokohama, Japan, pp. 109–114.

Cherchas, D. B., 1979, "A Dynamics Simulation for a High Speed Magnetically Levitated Guided Ground Vehicle," ASME JOURNAL OF DYNAMIC SYSTEMS, MEASUREMENT, AND CONTROL, Vol. 101, pp. 223–229.

Gran, R., 1990, "Benefits of Magnetically Levitated High Speed Transportation for the United States," SAE Future Transportation Conference, Paper No. 901475, San Diego, CA, Aug.

Gran, R., and Proise, M., 1993, "Five Degree of Freedom Analysis of the Grumman Superconducting Electromagnetic Maglev Vehicle Control/Guideway Interaction," Maglev 93 Conference, Argonne National Laboratory, May 19–21, Paper No. PS4-6.

Iskander, M. F., 1992, *Electromagnetic Fields and Waves,* Prentice-Hall, Englewood Cliffs, NJ.

Kalsi, S., Herbermann, R., Falkowski, C., Hennessy, M., and Bourdillon, A., 1993, "Magnet Design Optimization for Grumman Maglev Concept," Maglev 93 Conference, Argonne National Laboratory, May 19–21, Paper No. PS5-12.

Phelan, R. S., 1993, "High Performance Maglev Guideway Design," Doctoral Dissertation, Department of Civil Engineering, Massachusetts Institute of Technology, Jan.

Proise, M., Deutsch, L., Gran, R., Herbermann, R., Kalsi, S., and Shaw, P., 1993, "System Concept Definition of the Grumman Superconducting Electromagnetic Suspension (EMS) Maglev Design," Maglev 93 Conference, Argonne National Laboratory, May 19–21, Paper No. OS4-4.

Thornton, R. D., 1991, "Monorail Maglev Technology," *Electro International Conference Record,* New York, Apr. 16–18.

Wang, S. K., 1995, "Levitation and Guidance of a Maglev Vehicle Using Optimal Preview Control," Doctoral Dissertation, Department of Mechanical Engineering, Carnegie Mellon University, May.

Wormley, D. N., Thornton, R. D., Yu, S.-H., and Cheng, S., 1992, *Interactions Between Magnetically Levitated Vehicles and Elevated Guideway Structures,* U.S. Department of Transportation Technical Report DOT/FRA/NMI-92/23.